Antiferromagnetic order in CaK(Fe$_{1-x}$Ni$_x$)$_4$As$_4$ and its interplay with superconductivity

A. Kreyssig,[1,2] J. M. Wilde,[1,2] A. E. Böhmer,[1,2] W. Tian,[3] W. R. Meier,[1,2] Bing Li,[1,2] B. G. Ueland,[1,2] Mingyu Xu,[1,2]
S. L. Bud'ko,[1,2] P. C. Canfield,[1,2] R. J. McQueeney,[1,2] and A. I. Goldman[1,2]

[1]*Ames Laboratory, U.S. DOE, Ames, Iowa 50011, USA*
[2]*Department of Physics and Astronomy, Iowa State University, Ames, Iowa 50011, USA*
[3]*Neutron Scattering Division, Oak Ridge National Laboratory, Oak Ridge, Tennessee 37831, USA*

The magnetic order in CaK(Fe$_{1-x}$Ni$_x$)$_4$As$_4$ (1144) single crystals ($x = 0.051$ and 0.033) has been studied by neutron diffraction. We observe magnetic Bragg peaks associated with the same propagation vectors as found for the collinear stripe antiferromagnetic (AFM) order in the related BaFe$_2$As$_2$ (122) compound. The AFM state in 1144 preserves tetragonal symmetry and only a commensurate, noncollinear structure with a hedgehog spin-vortex crystal (SVC) arrangement in the Fe plane and simple AFM stacking along the *c* direction is consistent with our observations. The SVC order is promoted by the reduced symmetry in the FeAs layer in the 1144 structure. The long-range SVC order coexists with superconductivity, however, similar to the doped 122 compounds, the ordered magnetic moment is gradually suppressed with the developing superconducting order parameter. This supports the notion that both collinear and noncollinear magnetism and superconductivity are competing for the same electrons coupled by Fermi surface nesting in iron arsenide superconductors.

DOI: [10.1103/PhysRevB.97.224521](https://doi.org/10.1103/PhysRevB.97.224521)

The diversity of iron-based superconductors has provided many insights into the relationships between their structure, magnetism, and superconductivity. Iyo *et al.* [1] opened a new avenue of research with the discovery of the AeAFe$_4$As$_4$ ($Ae =$ Ca, Sr; $A =$ K, Rb, Cs) (1144) compounds. Although closely related to the much studied AeFe$_2$As$_2$ (122) families [2,3], there are important differences in their structure and symmetry. For example, the cation planes in CaKFe$_4$As$_4$ alternate between Ca and K as illustrated in Fig. 1. In consequence, there are two distinct As sites, As1 and As2, neighboring K and Ca, respectively, rather than one As site found in CaFe$_2$As$_2$ and KFe$_2$As$_2$. The local symmetry at the Fe sites is reduced from tetragonal to orthorhombic [1]. The space group for CaKFe$_4$As$_4$ is primitive tetragonal, $P4/mmm$, rather than body-centered tetragonal, $I4/mmm$, for CaFe$_2$As$_2$ and KFe$_2$As$_2$.

CaKFe$_4$As$_4$ shows bulk superconductivity below $T_c = 35$ K [1,4]. KFe$_2$As$_2$ is superconducting as well but with a dramatically lower $T_c \sim 3.8$ K [5]. In contrast, CaFe$_2$As$_2$ is not superconducting at ambient pressure and requires chemical substitution to realize superconductivity, e.g., electron doping by partially replacing Fe with Co or Ni or hole doping by substituting Na for Ca [6–8]. From this perspective of electron count, stoichiometric CaKFe$_4$As$_4$ may be viewed as nearly optimally hole-doped CaFe$_2$As$_2$, but without disorder arising from Ca and K randomly occupying the same site.

Partial substitution of Co or Ni for Fe in CaKFe$_4$As$_4$ (electron doping) should, in principle, shift the ground state from superconducting to antiferromagnetically (AFM) ordered [9]. Indeed, superconductivity is suppressed and signatures of an additional phase transition have been observed in electric resistance and specific heat measurements [10]. ^{57}Fe Mössbauer studies have revealed this additional phase transition to be magnetic in nature [10]. However, the orthorhombic lattice distortion that accompanies AFM in CaFe$_2$As$_2$ was not observed in CaK(Fe$_{1-x}$Ni$_x$)$_4$As$_4$ [10]. Furthermore, ^{75}As nuclear magnetic resonance (NMR) studies, together with symmetry analysis have proposed that the AFM order of the Fe moments is hedgehog spin-vortex crystal (SVC) order in the Fe planes as shown in Fig. 1(b). This order is characterized by noncollinear Fe moments featuring an alternating all-in and all-out motif around the As1 sites [10]. The temperature dependence of the nuclear spin-lattice relaxation rate provides evidence that the AFM order coexists microscopically with superconductivity [11].

Many open questions remain regarding the magnetic ordering in CaK(Fe$_{1-x}$Ni$_x$)$_4$As$_4$: What is the spatial extent of the correlations: long-range order or short-range? Is the magnetic order commensurate or incommensurate with the lattice? What is the nature of the magnetic correlations along the *c* direction: AFM or ferromagnetic (FM)? Is there an interplay between magnetism and superconductivity? Here we address the preceding questions via neutron diffraction measurements.

In this paper, we describe a neutron diffraction study of the magnetic order in electron-doped CaK(Fe$_{1-x}$Ni$_x$)$_4$As$_4$ single crystals with $x = 0.051$ and 0.033. In both samples, the Fe magnetic moments order antiferromagnetically in a long-range, commensurate, and noncollinear structure with a hedgehog spin-vortex crystal arrangement in the Fe planes and simple AFM stacking along the *c* direction. This magnetic order preserves the tetragonal symmetry and coexists with the superconductivity below T_c. For $x = 0.033$, the ordered magnetic moment is gradually suppressed below T_c. This is similar to the behavior observed for electron-doped Ba(Fe$_{1-x}M_x$)$_2$As$_2$ with $M =$ Co, Ni, or Rh [12–14] and hole-doped Ba$_{1-x}$K$_x$Fe$_2$As$_2$ [15] but contrasts with the mutual exclusion of AFM and superconductivity in electron-doped Ca(Fe$_{1-x}M_x$)$_2$As$_2$ [6,7,16].
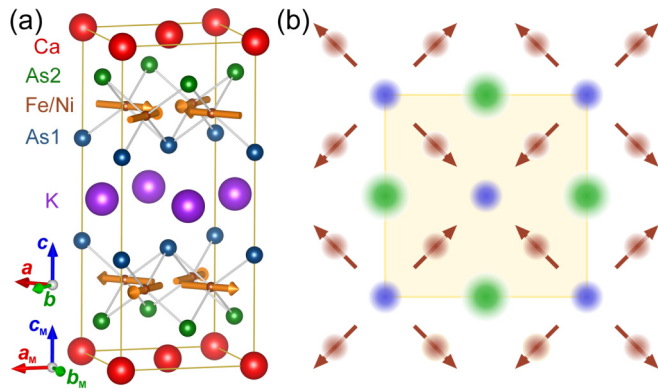
FIG. 1. Chemical and antiferromagnetic structure of $CaK(Fe_{1-x}Ni_x)_4As_4$. (a) Antiferromagnetic tetragonal unit cell with a_M, b_M, and c_M, which is doubled and 45° rotated in the (ab) plane with respect to the chemical unit cell with a, b, and c. The arrows represent the antiferromagnetically ordered Fe moments. (b) Arrangement of the magnetic Fe moments in a FeAs layer.

Single crystals of $CaK(Fe_{1-x}Ni_x)_4As_4$ with $x = 0.051(1)$ and $x = 0.033(1)$ and masses of 4.3(1) mg and 3.7(1) mg, respectively, were grown from a high-temperature transition-metal arsenic solution as described in Refs. [10,17]. Composition was determined via wavelength-dispersive x-ray spectroscopy employing a JEOL JXA-8200 microprobe system on cleaved surfaces of crystals from the same batches [17]. No deviation of the Ni concentrations outside of the given statistical error are observed for either batch. The AFM transition temperatures $T_N = 50.6(5)$ K and 42.9(5) K for $x = 0.051$ and 0.033, respectively, are inferred from temperature-dependent electrical-resistance and heat-capacity measurements using a Janis Research SHI-950T 4 Kelvin closed-cycle refrigerator and a Quantum Design (QD) Physical Property Measurement Systems. Employing a QD Magnetic Property Measurement System, no signatures of impurity phases were observed in magnetization measurements on the specific samples used in this study and T_c was determined to be 9.0(8) K and 21.0(4) K for $x = 0.051$ and 0.033, respectively. High-energy x-ray diffraction measurements similar to those described in Ref. [10] were performed on samples from the same batches and demonstrated that single crystals of both Ni concentrations maintain the same tetragonal crystallographic structure down to temperatures of 7 K.

Neutron diffraction measurements were performed on the HB-1A FIE-TAX triple-axis spectrometer at the High Flux Isotope Reactor, Oak Ridge National Laboratory, using a fixed incident energy of 14.6 meV, and effective collimations of $40'$-$40'$-S-$40'$-$80'$ in front of the pyrolytic graphite (PG) monochromator, between the monochromator and sample, between the sample and PG analyzer, and between the analyzer and detector, respectively. Two PG filters were used to minimize contamination from higher harmonics. The samples were mounted in a helium-filled aluminum can attached to the cold finger of a helium closed-cycle refrigerator with the (HHL) plane coincident with the scattering plane of the instrument. Both samples exhibited resolution-limited rocking scans indicating high-quality single crystals.
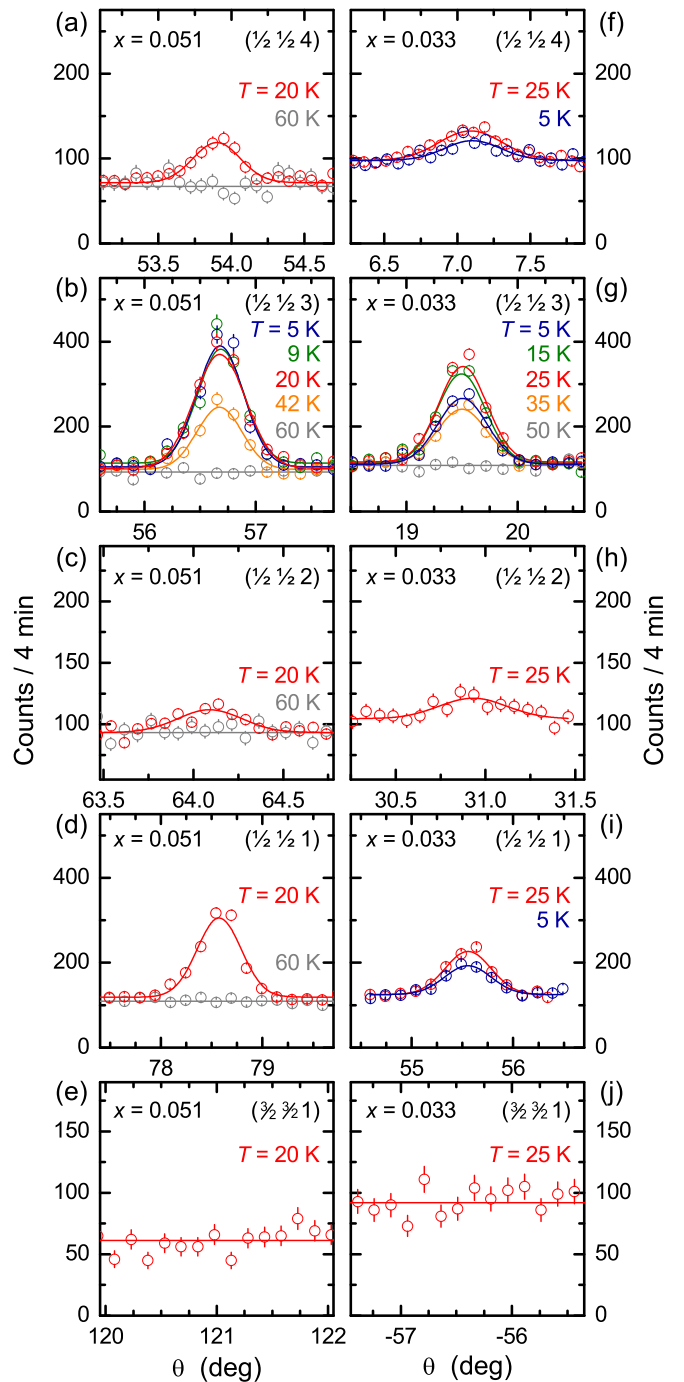

FIG. 2. Magnetic Bragg peaks of $CaK(Fe_{1-x}Ni_x)_4As_4$ measured by neutron diffraction rocking scans on single crystals with (a)–(e) $x = 0.051$ and (f)–(j) $x = 0.033$ at selected temperatures. The data are normalized to a monitor value of 240 mcu (monitor count units), which corresponds to 4 min of counting time.

Magnetic Bragg peaks at positions $(\frac{1}{2}\frac{1}{2}L)$ with integer L develop below the Néel temperature T_N as shown in Fig. 2. These Bragg peaks are consistent with AFM order characterized by a doubling, and 45° rotation, of the magnetic unit cell in the (ab) plane with respect to the chemical unit cell. Magnetic Bragg peaks at $(\frac{1}{2}\frac{1}{2}L)$ with half integer L are absent, as shown in Fig. 3, signaling that the magnetic and chemical unit cells have same lengths along c. Rocking scans through
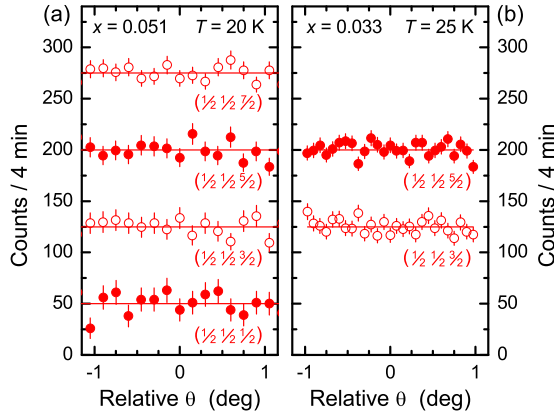
FIG. 3. Neutron diffraction rocking scans on CaK(Fe$_{1-x}$Ni$_x$)$_4$As$_4$ single crystals with (a) $x = 0.051$ and (b) $x = 0.033$ measured at AFM Bragg peak positions with half integer L associated with a unit cell doubling along c, and at a temperature well below T_N and slightly above T_c. The data are normalized to a monitor value of 240 mcu and are offset for clarity.

the AFM Bragg peaks displayed in Fig. 2 show the same shape and widths at all measured temperatures, as do scans through the $(\frac{1}{2}\frac{1}{2}3)$ AFM and the (112) nuclear Bragg peaks along the $(HH0)$ and $(00L)$ directions, as presented in Fig. 4. Taken together, these data demonstrate that the AFM Bragg peaks are resolution limited, which places a lower limit on the AFM correlation length of ~ 60 nm, and show that the AFM order is commensurate.

At first glance, the appearance of AFM Bragg peaks at (HHL) with half integer H and integer L might be attributed
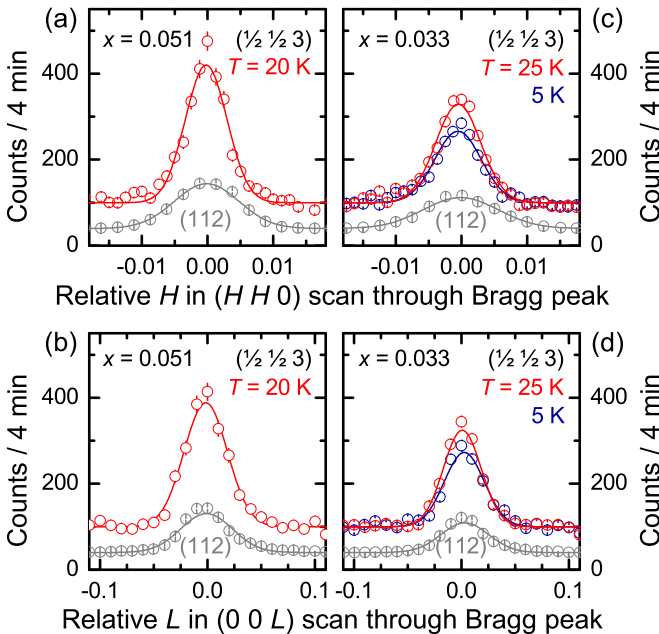

FIG. 4. Neutron diffraction scans along $(HH0)$ and $(00L)$ through the $(\frac{1}{2}\frac{1}{2}3)$ AFM Bragg peak for CaK(Fe$_{1-x}$Ni$_x$)$_4$As$_4$ single crystals with (a), (b) $x = 0.051$ and (c), (d) $x = 0.033$ and at selected temperatures. The data are normalized to a monitor value of 240 mcu. Similar scans through the (112) Bragg peak characterizing the chemical structure and the resolution conditions are shown for comparison with the intensity divided by a factor of 2000.

to the ubiquitous stripelike AFM in many other iron arsenides [3,18–20]. However, our evidence of a tetragonal unit cell in the AFM ordered phase is inconsistent with the orthorhombic distortion intrinsically linked to the stripelike AFM [13,20–24]. Alternatively, tetragonal AFM order can be constructed by coherent superposition of the two orientations of stripelike modulations [21–23,25–27]. These orientations arise from the pair of symmetry-equivalent propagation vectors $\tau_1 = (\pi, 0)$ and $\tau_2 = (0, \pi)$ in units of the Brillouin zone of the Fe square lattice.

Three different AFM arrangements of the Fe moments in the (ab) plane are distinguished by the relative orientation of the AFM ordered Fe-moment components μ_i to their corresponding propagation vectors τ_i: (i) μ_i in the (ab) plane and parallel to τ_i, (ii) μ_i in the (ab) plane and perpendicular to τ_i, and (iii) μ_i along the c direction [10,25,27–29]. These AFM structures have been described as (i) hedgehog SVC order, (ii) loops SVC order, and (iii) spin charge-density wave (SCDW) order [23,25,30] as illustrated in Fig. 1 of Ref. [10]. In each case, the AFM ordered Fe planes can be either AFM or FM stacked along c.

Table I compares the measured integrated intensities of selected AFM Bragg peaks to their intensities calculated using FULLPROF [31] for each of these six cases. Qualitative comparison of intensities between the different columns yields the result that only the hedgehog SVC order with AFM stacking along the c direction is consistent with the observations for both samples, e.g., the $(\frac{1}{2}\frac{1}{2}3)$ Bragg peaks are the strongest and the $(\frac{3}{2}\frac{3}{2}1)$ Bragg peaks are very weak for both samples and this AFM order. This hedgehog SVC order is consistent with the arrangement of the Fe moments in the (ab) plane proposed by Meier *et al.* [10] and is illustrated in Fig. 1. The magnetic space group is $P_C 4/mbm$ (BNS) with respect to the AFM unit cell [32], and $P_P 4'/mmm'$ (OG) with respect to the chemical unit cell [33]. The AFM order can be described as a two-τ structure with propagation vectors $\tau_1 = (\pi, 0)$ and $\tau_2 = (0, \pi)$, or $\tau_1 = (\frac{1}{2}\frac{1}{2}1)$, and $\tau_2 = (\frac{\bar{1}}{2}\frac{1}{2}1)$ in reciprocal lattice units, modulating Fe moments μ_i in the (ab) plane with $\mu_i \parallel \tau_i$.

From fitting the measured integrated intensities of the AFM Bragg peaks listed in Table I against the calculated values for this hedgehog SVC structure, the total AFM ordered moment per transition-metal site is determined as 0.37(10) μ_B and 0.34(10) μ_B for the $x = 0.051$ sample at $T = 20$ K and the $x = 0.033$ sample at $T = 25$ K, respectively. The value for $x = 0.051$ is in good agreement with the hyperfine field at the Fe position determined from ^{57}Fe Mössbauer measurements [10].

Figure 5 shows the temperature dependence of the intensity measured at the $(\frac{1}{2}\frac{1}{2}3)$ AFM Bragg peak position for both samples, which is proportional to the square of the AFM moment, the AFM order parameter. The AFM ordering for both samples is well described as a second-order phase transition by a power law with $T_N = 50.0(4)$ K and 41.8(4) K for the $x = 0.051$ and $x = 0.033$ samples, respectively, in agreement with results from the transport and thermodynamic measurements described earlier. The critical exponent for both samples is $\beta = 0.29(2)$, which is close to the value of 0.33 expected for a three-dimensional Heisenberg system. This behavior is consistent with the fact that the 1144 structure already features

TABLE I. Integrated intensity of selected AFM Bragg peaks measured on both $CaK(Fe_{1-x}Ni_x)_4As_4$ single crystals and calculated for a total magnetic moment of 0.37 μ_B per transition-metal site for the SVC orders, and alternating 0.74 μ_B and 0 μ_B per transition-metal site for the SCDW order. The intensities are in arbitrary units and normalized to the intensities of ten selected chemical Bragg peaks.

	Measurement		Calculation					
	$x = 0.033$	$x = 0.051$	Hedgehog SVC in (ab) plane: $\mu_i \parallel \tau_i$		Loops SVC in (ab) plane: $\mu_i \perp \tau_i$		SCDW $\mu_i \parallel c$	
AFM Bragg peak	$T = 25$ K	$T = 20$ K	AFM along c	FM along c	AFM along c	FM along c	AFM along c	FM along c
$(\frac{1}{2}\frac{1}{2}4)$	22	18	19	80	26	107	13	54
$(\frac{1}{2}\frac{1}{2}3)$	143	144	130	17	207	26	155	20
$(\frac{1}{2}\frac{1}{2}2)$	12	6	9	164	21	384	24	441
$(\frac{1}{2}\frac{1}{2}1)$	69	95	99	1	634	8	1071	14
$(\frac{3}{2}\frac{3}{2}1)$	<2	<2	1	0.1	32	0.4	63	1

the necessary broken structural symmetry, which allows for the onset of the hedgehog SVC order to be second order.

As the temperature is lowered below the superconducting transition temperature, T_c, AFM order persists and coexists with superconductivity in $CaK(Fe_{1-x}Ni_x)_4As_4$. For $x = 0.051$, the AFM order parameter increases smoothly to the lowest temperature measured. However, for $x = 0.033$, the magnetic order parameter clearly decreases gradually below T_c. This is reminiscent of what has been observed for $Ba(Fe_{1-x}M_x)_2As_2$ with $M =$ Co, Ni, and Rh [12–14], and $Ba_{1-x}K_xFe_2As_2$ [15]. The $CaK(Fe_{1-x}Ni_x)_4As_4$ series is

FIG. 5. Temperature dependence of the intensity of the $(\frac{1}{2}\frac{1}{2}3)$ AFM Bragg peak for $CaK(Fe_{1-x}Ni_x)_4As_4$ single crystals with $x = 0.051(1)$ and $x = 0.033(1)$. The measured counts represent the intensity because the widths of the AFM Bragg peaks do not change with temperature. The data are offset for clarity and normalized to the mass of the sample and a monitor value of 240 mcu. The lines represent power-law fits as described in the text. The transition temperatures are marked by arrows at values for T_N determined from the fits and for T_c determined from magnetization measurements.

the second example of such coexistence and competition in iron-based superconductors but with a different AFM order.

The 1144 compounds fill a unique and interesting niche in the family of iron-based superconductors due to the reduced symmetry in the FeAs layers. In most iron-based superconductors, the Fe site has tetragonal symmetry and a high-symmetry direction can be found every 45° in the (ab) plane, e.g., the a, b, and diagonal directions. In contrast, the Fe site has orthorhombic symmetry in the 1144 compounds with high-symmetry directions only every 90°. In this environment, magnetocrystalline anisotropy and spin-orbit coupling constrain the Fe magnetic moments to lie in these high-symmetry directions which is exemplified by the SVC motif in Fig. 1. In contrast, if stripe-type AFM were to occur, the Fe moments would lie along arbitrary directions. This leads to a preference for SVC orders in 1144 compounds [25–27].

In both, the 1144 and 122 compounds, the AFM orders are related to the same propagation vector $(\pi,0)$ and the symmetry equivalent $(0,\pi)$ but with different directions for the AFM ordered Fe moments. In the 1144 compounds, the Fe moments are arranged in the noncollinear SVC motif and lie 45° to those of the collinear stripelike order in the 122 system. However, both AFM orders demonstrate a similar interplay with superconductivity. This suggests that whereas their common underling propagation vectors may be important, the orientation of the ordered moments and their collinear or noncollinear arrangement apparently are not. So, as an example, the scattering of superconducting electron pairs by magnetic moments, which would be expected to change for different moment directions and (non)collinearity, seems not to be a dominating factor for the interplay between superconductivity and AFM. Instead it points to superconductivity and magnetism competing for the same electrons coupled by the same wave vector, i.e., the Fermi surface nesting vector $(\pi,0)$ [12]. Hereby, the AFM order plays the role of an intrinsic Josephson coupling and provides a sensitive probe of the relative phase of the superconducting pair wave functions [12]: Whereas a pairing mechanism with s^{++} symmetry is intrinsically unsuitable for coexistence of superconductivity
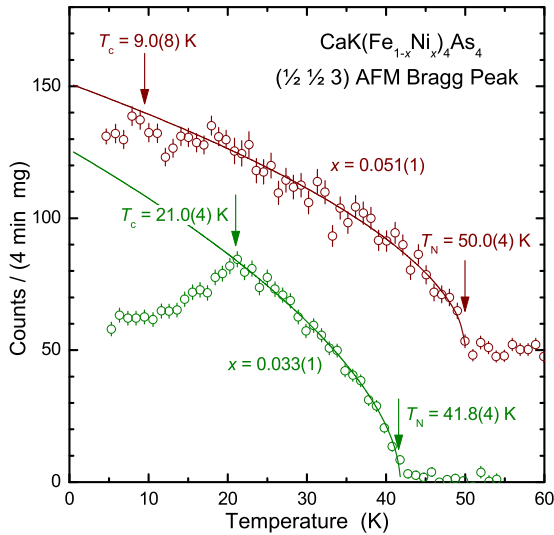
with AFM, an s^{+-} state may or may not coexist with AFM depending on the details of the band structure. The observed coexistence and competition revealed by the gradual suppression of the ordered magnetic moment below T_c strongly supports a pairing mechanism with s^{+-} symmetry in the 1144 system consistent with the two-gap $s + s$ model deduced from muon spectroscopy [34] and the two-gap s^{+-} superconductivity concluded from penetration depth and tunneling conductance measurements [35,36], and as has previously been established for the 122 iron-arsenide superconductors [12,26].

Summarizing, we have shown via neutron diffraction measurements that the magnetic order in CaK(Fe$_{1-x}$Ni$_x$)$_4$As$_4$ is long range and commensurate to the lattice. The Fe moments order in a hedgehog SVC motif in each Fe plane and are AFM stacked along the ***c*** direction. The 1144 compounds are unique in the family of iron-based superconductors due to the reduced symmetry in the FeAs layers promoting SVC order. This noncollinear AFM order coexists with superconductivity,

however, the magnetic order parameter decreases gradually below T_c, reminiscent of what has previously been observed for collinear stripelike AFM in 122 compounds.

[1] A. Iyo, K. Kawashima, T. Kinjo, T. Nishio, S. Ishida, H. Fujihisa, Y. Gotoh, K. Kihou, H. Eisaki, and Y. Yoshida, J. Am. Chem. Soc. **138**, 3410 (2016).

[2] P. C. Canfield and S. L. Bud'ko, Annu. Rev. Condens. Matter Phys. **1**, 27 (2010).

[3] J. Paglione and R. L. Greene, Nature Phys. **6**, 645 (2010).

[4] W. R. Meier, T. Kong, U. S. Kaluarachchi, V. Taufour, N. H. Jo, G. Drachuck, A. E. Böhmer, S. M. Saunders, A. Sapkota, A. Kreyssig *et al.*, Phys. Rev. B **94**, 064501 (2016).

[5] K. Sasmal, B. Lv, B. Lorenz, A. M. Guloy, F. Chen, Y.-Y. Xue, and C.-W. Chu, Phys. Rev. Lett. **101**, 107007 (2008).

[6] S. Ran, S. L. Bud'ko, W. E. Straszheim, J. Soh, M. G. Kim, A. Kreyssig, A. I. Goldman, and P. C. Canfield, Phys. Rev. B **85**, 224528 (2012).

[7] S. Ran, S. L. Bud'ko, W. E. Straszheim, and P. C. Canfield, Phys. Rev. B **90**, 054501 (2014).

[8] K. Zhao, Q. Q. Liu, X. C. Wang, Z. Deng, Y. X. Lv, J. L. Zhu, F. Y. Li, and C. Q. Jin, J. Phys.: Condens. Matter **22**, 222203 (2010).

[9] V. Zinth, T. Dellmann, H.-H. Klauss, and D. Johrendt, Angew. Chem. Int. Ed. **50**, 7919 (2011).

[10] W. R. Meier, Q.-P. Ding, A. Kreyssig, S. L. Bud'ko, A. Sapkota, K. Kothapalli, V. Borisov, R. Valenti, C. D. Batista, P. P. Orth *et al.*, npj Quant. Mat. **3**, 5 (2018).

[11] Q.-P. Ding, W. R. Meier, A. E. Böhmer, S. L. Bud'ko, P. C. Canfield, and Y. Furukawa, Phys. Rev. B **96**, 220510(R) (2017).

[12] R. M. Fernandes, D. K. Pratt, W. Tian, J. Zarestky, A. Kreyssig, S. Nandi, M. G. Kim, A. Thaler, N. Ni, P. C. Canfield *et al.*, Phys. Rev. B **81**, 140501(R) (2010).

[13] A. Kreyssig, M. G. Kim, S. Nandi, D. K. Pratt, W. Tian, J. L. Zarestky, N. Ni, A. Thaler, S. L. Bud'ko, P. C. Canfield *et al.*, Phys. Rev. B **81**, 134512 (2010).

[14] H. Luo, R. Zhang, M. Laver, Z. Yamani, M. Wang, X. Lu, M. Wang, Y. Chen, S. Li, S. Chang *et al.*, Phys. Rev. Lett. **108**, 247002 (2012).

[15] J. Munevar, H. Micklitz, J. Agüero, G. Tan, C. Zhang, P. Dai, and E. Baggio-Saitovitch, Phys. Rev. B **88**, 184514 (2013).

[16] A. Sapkota, P. Das, A. E. Böhmer, B. G. Ueland, D. L. Abernathy, S. L. Bud'ko, P. C. Canfield, A. Kreyssig, A. I. Goldman, and R. J. McQueeney, Phys. Rev. B **97**, 174519 (2018).

[17] W. R. Meier, T. Kong, S. L. Bud'ko, and P. C. Canfield, Phys. Rev. Mater. **1**, 013401 (2017).

[18] M. D. Lumsden and A. D. Christianson, J. Phys.: Condens. Matter **22**, 203203 (2010).

[19] P. Dai, Rev. Mod. Phys. **87**, 855 (2015).

[20] A. I. Goldman, D. N. Argyriou, B. Ouladdiaf, T. Chatterji, A. Kreyssig, S. Nandi, N. Ni, S. L. Bud'ko, P. C. Canfield, and R. J. McQueeney, Phys. Rev. B **78**, 100506(R) (2008).

[21] M. G. Kim, A. Kreyssig, A. Thaler, D. K. Pratt, W. Tian, J. L. Zarestky, M. A. Green, S. L. Bud'ko, P. C. Canfield, R. J. McQueeney *et al.*, Phys. Rev. B **82**, 220503(R) (2010).

[22] F. Waßer, A. Schneidewind, Y. Sidis, S. Wurmehl, S. Aswartham, B. Büchner, and M. Braden, Phys. Rev. B **91**, 060505(R) (2015).

[23] J. M. Allred, K. M. Taddei, D. E. Bugaris, M. J. Krogstad, S. H. Lapidus, D. Y. Chung, H. Claus, M. G. Kanatzidis, D. E. Brown, J. Kang *et al.*, Nature Phys. **12**, 493 (2016).

[24] S. Nandi, M. G. Kim, A. Kreyssig, R. M. Fernandes, D. K. Pratt, A. Thaler, N. Ni, S. L. Bud'ko, P. C. Canfield, J. Schmalian *et al.*, Phys. Rev. Lett. **104**, 057006 (2010).

[25] V. Cvetkovic and O. Vafek, Phys. Rev. B **88**, 134510 (2013).

[26] R. M. Fernandes, A. V. Chubukov, and J. Schmalian, Nature Phys. **10**, 97 (2014).

[27] J. O'Halloran, D. F. Agterberg, M. X. Chen, and M. Weinert, Phys. Rev. B **95**, 075104 (2017).

[28] M. H. Christensen, J. Kang, B. M. Andersen, I. Eremin, and R. M. Fernandes, Phys. Rev. B **92**, 214509 (2015).

[29] R. M. Fernandes, S. A. Kivelson, and E. Berg, Phys. Rev. B **93**, 014511 (2016).

[30] X. Wang, J. Kang, and R. M. Fernandes, Phys. Rev. B **91**, 024401 (2015).

[31] J. Rodgriguez-Carvajal, Physica B **192**, 55 (1993).

[32] N. V. Belov, N. N. Neronova, and T. S. Smirnova, Trudy Inst. Kristall. Acad. SSSR **11**, 33 (1955).

[33] W. T. Opechowski and R. Guccione, *Magnetism*, edited by G. T. Rado and H. Suhl, Vol. II, Part A (Academic Press, New York, 1965).

[34] P. K. Biswas, A. Iyo, Y. Yoshida, H. Eisaki, K. Kawashima, and A. D. Hillier, Phys. Rev. B **95**, 140505 (2017).

[35] K. Cho, A. Fente, S. Teknowijoyo, M. A. Tanatar, K. R. Joshi, N. M. Nusran, T. Kong, W. R. Meier, U. Kaluarachchi, I. Guillamón, H. Suderow, S. L. Bud'ko, P. C. Canfield, and R. Prozorov, Phys. Rev. B **95**, 100502(R) (2017).

[36] S. Teknowijoyo, K. Cho, M. Kończykowski, E. I. Timmons, M. A. Tanatar, W. R. Meier, M. Xu, S. L. Bud'ko, P. C. Canfield, and R. Prozorov, Phys. Rev. B **97**, 140508(R) (2018).